Acta Cryst B
STRUCTURAL SCIENCE
CRYSTAL ENGINEERING
MATERIALS
ISSN 2052-5206

Pressure-induced structural phase transformation in cobalt(II) dicyanamide

Andrey A. Yakovenko, Karena W. Chapman and Gregory J. Halder*

X-ray Science Division, Advanced Photon Source, Argonne National Laboratory, 9700 S Cass Ave, Argonne, Illinois 60439, USA. *Correspondence e-mail: halder@aps.anl.gov

Received 6 February 2015
Accepted 23 March 2015

Edited by A. J. Blake, University of Nottingham, England

Keywords: high pressure; magnetic molecular framework material; MOFs.

CCDC references: 1055794; 1055795; 1055796; 1055797; 1055798; 1055799; 1055800; 1055801; 1055802

Supporting information: this article has supporting information at journals.iucr.org/b

In situ synchrotron powder diffraction has been used to probe the pressure-dependent structural properties of the magnetic molecular framework material $Co(dca)_2$ [dca = dicyanamide or $N(CN)_2^-$]. An orthorhombic (*Pmnn*) to monoclinic ($P2_1/n$) transformation to a high-pressure phase, namely γ-$Co(dca)_2$, occurs at 1.1 GPa. Structural determination of γ-$Co(dca)_2$ shows that the rutile-like topology of the pristine material is retained at high pressures, with the lower symmetry allowing a progression of volume-reducing structural distortions. γ-$Co(dca)_2$ was stable at the maximum pressure measured of 4.2 GPa. Both phases were soft, with bulk moduli (B_0) for α-$Co(dca)_2$ and γ-$Co(dca)_2$ of 13.15 (18) and 9.0 (6) GPa, respectively. Modest uniaxial negative linear compressibility (K) of the order of -4 TPa^{-1} was observed over the entire measured pressure range.

1. Introduction

Pressure offers a novel means to perturb the structure and function of molecular materials, including molecular magnets and metal–organic frameworks (MOFs; Tan & Cheetham, 2011). The rich structural chemistry and complex topologies of these materials can give rise to more unusual pressure-induced behaviour than traditional solid-state materials (*e.g.* metal oxides and intermetallics) more commonly explored under high-pressure conditions (Halder *et al.*, 2011; Chapman *et al.*, 2008; Lapidus *et al.*, 2013; Graham *et al.*, 2011; Ogborn *et al.*, 2012; Bennett *et al.*, 2011). For instance, the structurally simple molecular material $Zn(CN)_2$ exhibits a diverse range of pressure-induced transformations, most significantly a pronounced dependence on the fluid used to transmit hydrostatic pressure whereby small molecule fluids can trigger major structural rearrangements. The typically flexible and low density nature of molecular materials allows access to such pressure-induced phenomena under relatively mild conditions, such as could be routinely encountered in practical applications. This has been demonstrated for the nanoporous MOF system ZIF-8 [Zn(2-methylimidazolate)$_2$], where the porosity of the system is irreversibly modified following a crystalline-amorphous transition during pelletization (< 0.5 GPa) to optimize volumetric gas storage capacity (Chapman *et al.*, 2009, 2011). To this end, thorough examination of their pressure-dependent structures represents a critical step in the advancement of the field toward a diverse range of important applications (Furukawa *et al.*, 2013).

The topological versatility of molecular framework materials, whereby magnetically active metal centres can be connected into regular networks, underlies a wide range of interesting magnetic and electronic properties (Kurmoo, 2009). For example, frameworks constructed from transition

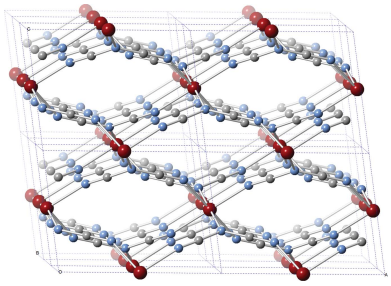

metals bridged by dicyanamide anions (dca) represent an important class of molecular magnet. The isostructural series of non-porous materials with rutile-like frameworks [referred to as α-$M^{II}(dca)_2$, where M = Mn, Fe, Co, Ni, Cu] consisting of octahedral metal centres bridged by three-connecting dca ligands. This family exhibits a diverse range of magnetic ground states, from paramagnetic [α-Cu(dca)$_2$] to ferromagnetic [α-Co(dca)$_2$, α-Ni(dca)$_2$] and antiferromagnetic [α-Mn(dca)$_2$, α-Fe(dca)$_2$], and in some cases undergo long-range magnetic ordering transitions at low temperatures (Batten *et al.*, 1998; Kurmoo & Kepert, 1998). The layered polymorphs β-$M^{II}(dca)_2$ (M = Co, Zn), consisting of tetrahedrally coordinated metal centres bridged by two-connecting dca ligands (Köhler, 1964; Jensen *et al.*, 1999), are only known to be generated *via* alternative synthetic routes. β-Co(dca)$_2$ is a spin-canted antiferromagent.

The atomic structure of the magnetic molecular framework material α-Co(dca)$_2$ was first reported from analysis of ambient-pressure single-crystal X-ray diffraction data (Kurmoo & Kepert, 1998). Chains of Co^{II} octahedra aligned parallel to the *a* direction are bridged by pairs of ligands, equatorially coordinated through the terminal nitrogen atoms [*i.e.* $\cdots$Co$-$(N$\equiv$C$-$N$-$C$\equiv$N)$_2-$Co$\cdots$, Fig. 1]. Adjacent chains are offset in the *c* direction allowing the apical amide N atoms of the ligands to coordinate to the axial positions of the Co^{II} octahedra. The resulting highly connected framework structure has a rutile-like topology (six-connecting metal nodes bridged by three-connecting ligands), where the asymmetry of the three-connecting node reduces the crystal symmetry to orthorhombic (*cf.* the tetragonal symmetry of the archetypal rutile structure; Anthony *et al.*, 2001). A crystallographic study of how this structure responds to high pressure has not been previously explored.

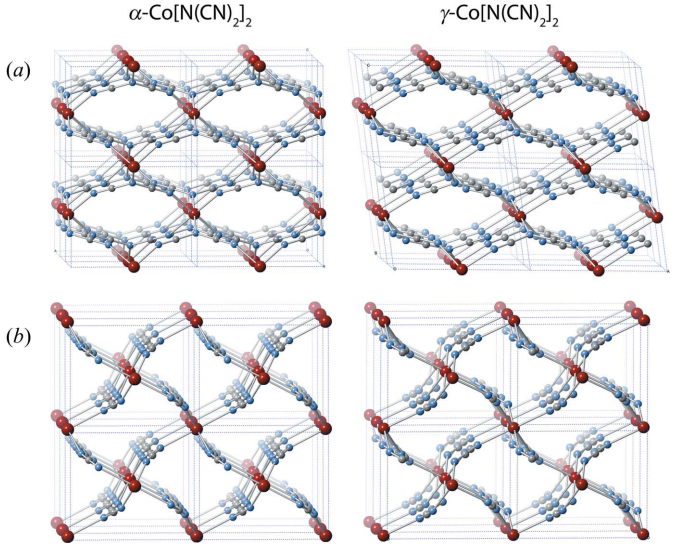

Figure 1
Representations of the crystal structures for α-Co(dca)$_2$ at $\sim$0.4 GPa (left) and γ-Co(dca)$_2$ at $\sim$3.6 GPa (right): (*a*) side- and (*b*) end-on perspectives of the doubly bridged $\cdots$Co$-$(NC$-$N$-$CN)$_2-$Co$\cdots$ chains (as viewed down the [010] and [100] directions, respectively).

In earlier work, magnetic and vibrational spectroscopy measurements at elevated pressures have been used to investigate several members of the α-$M^{II}(dca)_2$ family. The magnetic properties of α-Fe(dca)$_2$, α-Co(dca)$_2$ and α-Ni(dca)$_2$ were studied up to $\sim$2 GPa using AC susceptibility measurements, with each showing different pressure-dependent behaviour despite the isostructural relationship of the ambient pressure phases (Nuttall *et al.*, 2000). For α-Fe(dca) the Néel temperature increases continuously with increasing pressure, while the Curie temperature for α-Ni(dca)$_2$ shows an initial increase with pressure but then remains relatively constant above 0.2 GPa. Most notably, α-Co(dca)$_2$ shows a magnetic crossover from ferromagnetic to antiferromagnetic behaviour near 1 GPa. More recently, the local lattice distortions for α-Co(dca)$_2$ were probed using high-pressure IR and Raman spectroscopy (Musfeldt *et al.*, 2013). This work reported pressure-driven changes to the vibration modes at approximately 1 and 3 GPa; the first being attributed to a major symmetry-lowering transition ['γ-Co(dca)$_2$'], and the second to a more modest structural change ['δ-Co(dca)$_2$'].

Here we present a high-pressure crystallographic study of α-Co(dca)$_2$, including the structural determination of the high-pressure phase γ-Co(dca)$_2$. The pressure-dependence of the atomic structure was probed within a diamond–anvil cell using synchrotron-based powder diffraction methods.

2. Materials and methods

A polycrystalline sample of α-Co(dca)$_2$ was prepared as described previously (Kurmoo & Kepert, 1998). High-pressure powder diffraction data for α-Co(dca)$_2$ were measured within a diamond–anvil cell (DAC) pressure apparatus. A carefully ground sample was loaded into the 300 µm diameter hole in a stainless steel gasket of 250 µm thickness pre-indented to 100 µm thickness within a DAC (Diacell Bragg-G) equipped with 500 µm culet anvils. Polycrystalline NaCl ($\sim$10% by volume) was included as an internal pressure marker, and isopropanol was used to mediate hydrostatic compression (hydrostatic limit: 4.2 GPa; Piermarini, 1973). *In-situ* high-pressure diffraction data were collected using the monochromatic X-rays available at the 1-BM (20.052 keV, 0.61832 Å) and 17-BM (16.529 keV, 0.75009 Å) beamlines (100 µm diameter beam size) at the Advanced Photon Source, Argonne National Laboratory, in combination with either a mar345 imaging-plate detector or a Perkin–Elmer amorphous-Si flat panel detector. Diffraction data were collected every 0.1–0.2 GPa in the range 0–4.2 GPa, and also during the gradual release of pressure. The raw images were processed within *FIT-2D* (Hammersley *et al.*, 1996), refining the sample-to-detector distance and tilt of the detector relative to the beam based on data obtained for a LaB_6 standard. Indexing of a new high-pressure phase was undertaken within GSAS-II (Toby & Von Dreele, 2013). Structural parameters were evaluated by Rietveld fits to the diffraction data within *JANA*2006 (Petříček *et al.*, 2006). Additional details for the Rietveld refinements, including difference profiles, are included in the supporting information. The sample pressure

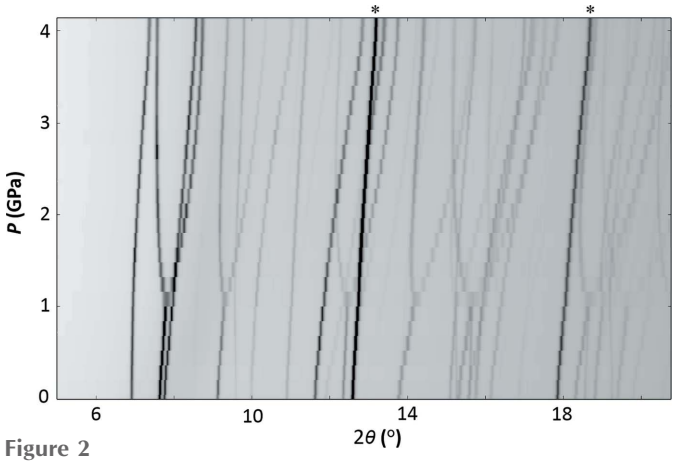

Figure 2
Diffraction data upon compression in isopropanol showing the symmetry-lowering phase transition at 1.1 GPa. The strong peaks at ∼13° and ∼18° (*) arise from the NaCl internal pressure standard. Intensity is scaled from light grey (no/low intensity) to black (highest intensity).

was determined based on the refined lattice volume for the NaCl internal diffraction standard with known compressibility (Decker, 1971). Bulk moduli (B_0) and linear compressibility (K) values were evaluated using the *PASCal* program (Cliffe & Goodwin, 2012).

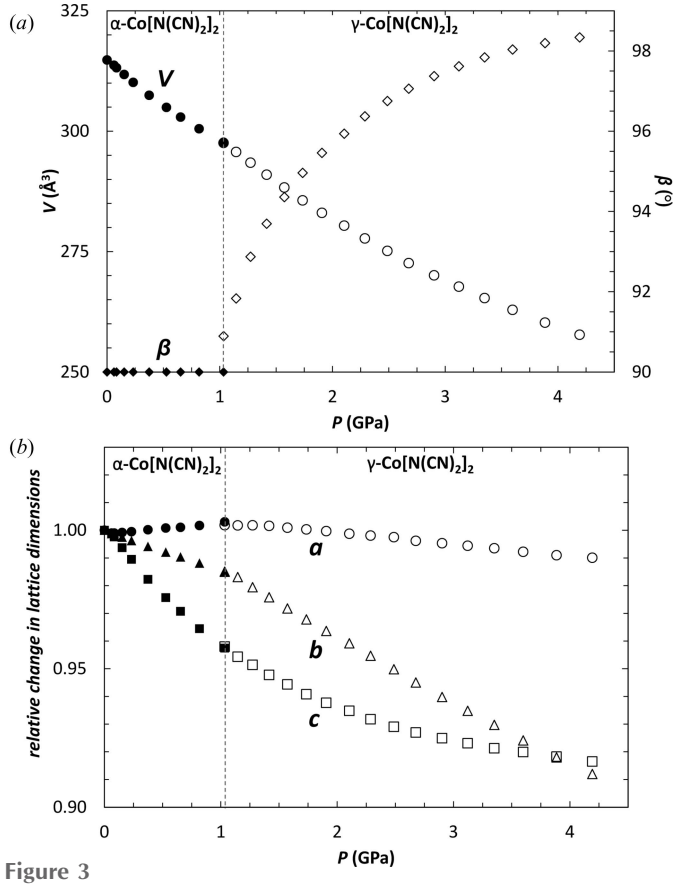

Figure 3
(*a*) Pressure dependence of the lattice volume (V) and β-angle for α-Co(dca)$_2$ (solid markers) and γ-Co(dca)$_2$ (hollow markers). (*b*) Relative change in the lattice dimensions (a, b and c) as a function of pressure. Vertical dashed lines indicated transition pressure where two phases are present. Errors are within the size of the data points.

3. Results

The diffraction data exhibit a second-order structural phase transition at 1.1 GPa (Fig. 2) that is reversible upon release of pressure (Fig. S1). The transition was characterized by a splitting of Bragg peaks, suggesting a symmetry lowering from the parent orthorhombic structure (*Pmnn*). This is consistent with the first transition pressure observed in vibrational spectroscopy studies, and for consistency with this earlier work we will also refer to it as the γ-Co(dca)$_2$ phase. This high-pressure phase was found to have a monoclinic lattice closely related to α-Co(dca)$_2$, where $a \simeq a'$, $b \simeq b'$, $c \simeq c'$, $\beta \simeq 90°$, and with systematic absences consistent with the space group $P2_1/n$. Variations in lattice parameters for both phases, determined from Rietveld fits (Fig. S2) to the high-pressure diffraction data, are plotted in Fig. 3. Key structural parameters are plotted in Fig. 4 and Fig. S6. Refinement and crystal structure details are included in Table S1.

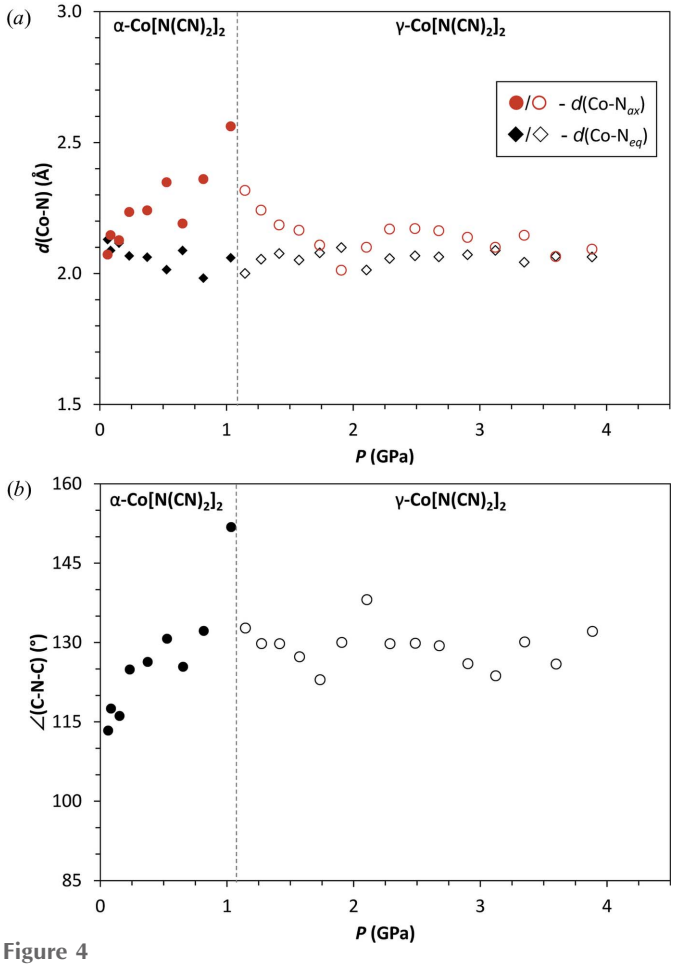

Figure 4
Pressure dependence of (*a*) the Co—N bond lengths and (*b*) the amide C—N—C bond angles for α-Co(dca)$_2$ (solid markers) and γ-Co(dca)$_2$ (hollow markers). The different Co—N bond lengths are shown in red (axial, amide nitrogen) and black (equatorial, cyanide nitrogen) to highlight the elongation of the Co^{II} octahedral in α-Co(dca)$_2$. For γ-Co(dca)$_2$ the average of the two unique Co—N$_{eq}$ bond lengths are shown. Vertical dashed lines indicate transition pressure. Error bars are within the size of the data points.

The initial atomic coordinates for the refinement of γ-Co(dca)$_2$ at 4.2 GPa were generated from the parent α-Co(dca)$_2$ structure (Fig. 4*a*). The coordinates were subsequently optimized by applying the non-linear Marquardt technique (Marquardt, 1963), allowing the atomic structure to adapt to the new symmetry settings. To alleviate chemically unreasonable dca geometries across all pressures, the following bond length and angle restraints were applied: C≡N to ∼1.15 Å, C—N to ∼1.32 Å and N—C≡N angles to ∼180°. These restraints are generally consistent with features that showed only pressure-induced broadening in vibrational spectroscopy measurements (Musfeldt *et al.*, 2013). The structures of γ-Co(dca)$_2$ at lower pressures were refined sequentially using parameters from the 4.2 GPa structure as the initial model in the refinement series.

The structure of γ-Co(dca)$_2$ at 3.6 GPa is presented in Fig. 1 and Fig. 5. While the connectivity of the framework atoms is unchanged for γ-Co(dca)$_2$ compared with α-Co(dca)$_2$, several major changes are clearly evident. Among the most significant is the deviation in the β-angle that defines an offset in the *ABAB* stacking of chains, as shown in Fig. 1(*a*). A second important change is that the two CN groups of the ligand become crystallographically independent allowing for subtle differences in their binding geometries and rotation of the Co^{II} octahedral (Fig. 5). Further structural details are discussed below (§4.2).

4. Discussion

4.1. Compression mechanics

The lattice dimensions for α-Co(dca)$_2$ show marked anisotropy under compression, where the orthorhombic symmetry of the framework induces 'wine-rack'-like structural mechanics. Compression in the *b* and *c* directions, that are associated with inter-chain packing, causes an expansion in the *a* direction whereby the Co^{II} centres along the chain are forced further apart (Fig. S3). Negative linear compressibility (NLC) is a relatively rare phenomenon, with some of the largest reported NLC occurring in molecular framework materials (Cairns *et al.*, 2013). The NLC value (K_a) for α-Co(dca)$_2$ *a*-axis is −3.7 (3) TPa^{-1} (see Fig. S4), which is comparable to that of the molecular framework [NH$_4$][Zn(HCOO)$_3$] (−1.8 TPa^{-1}; Li *et al.*, 2012), but significantly smaller than the 'giant' effect observed in some cyanide-bridged frameworks (*e.g.* −76 TPa^{-1} for the low-pressure phase of Ag$_3$[Co(CN)$_6$]; Goodwin *et al.*, 2008). Considering the overall pressure response of the α-Co(dca)$_2$ lattice, the NLC effect of the *a*-axis is outweighed by much larger positive contributions in the other two directions [K_b = 14.2 (3) and K_c = 46.6 (4) TPa^{-1}] resulting in a relatively soft material with a bulk modulus of B_0 = 13.15 (18) GPa [B' = 11.8 (5)]. This is within the range of previously reported bulk moduli for cyanide-bridged molecular materials {*e.g.* B_0 = 6.5 (3), 16.7 (16) and 34.49 (22) GPa for Ag$_3$[Co(CN)$_6$], Zn[Au(CN)$_2$]$_2$ and Zn(CN)$_2$}.

The lattice volume compresses continuously for the entire pressure range studied (0–4.2 GPa), consistent with the second-order nature of the α-Co(dca)$_2$ to γ-Co(dca)$_2$ transition (Fig. 3*a*). The increased degrees of structural flexibility afforded by the lower symmetry of γ-Co(dca)$_2$ allows for larger structural distortions compared to α-Co(dca)$_2$, resulting in a significantly softer material with a bulk modulus of B_0 = 9.0 (6) GPa [B' = 11.8 (5)]. Notably, γ-Co(dca)$_2$ is stable up to 4.2 GPa, confirming that previously observed local structure changes above 3 GPa [attributed to a 'δ-Co(dca)$_2$' phase] are not associated with long-range

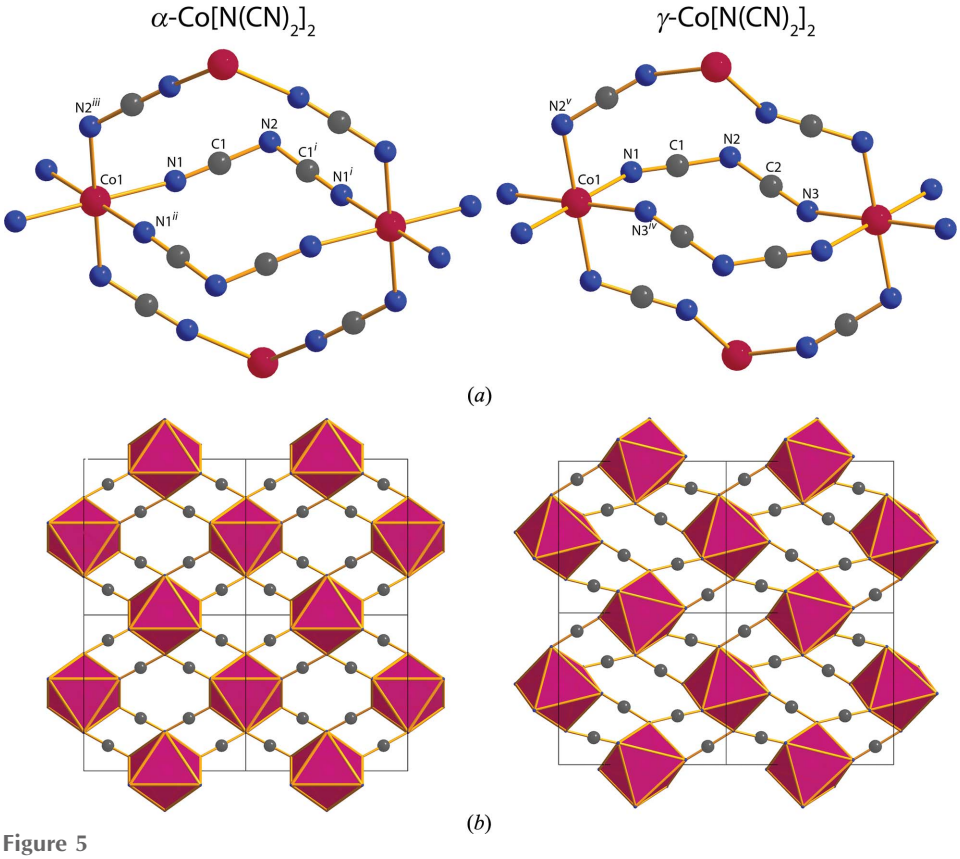

Figure 5
Representations of the crystal structures for α-Co(dca)$_2$ at ∼0.4 GPa and γ-Co(dca)$_2$ at ∼3.6 GPa. (*a*) Close-up view of the metal–ligand connectivity between four nearest-neighbour Co^{II} centres with atoms from the asymmetric units labelled accordingly. (*b*) Co^{II} octahedral packing diagrams as viewed in the (001) plane. C and N atoms are displayed as balls and sticks, respectively, for clarity. Symmetry codes: (i) $-x, y, z$; (ii) $x, -y, -z$; (iii) $\frac{1}{2}-x, -\frac{1}{2}+y, -\frac{1}{2}-z$; (iv) $-x, -y, -z$; (v) $\frac{1}{2}+x, \frac{1}{2}-y, \frac{1}{2}+z$.

crystallographic order (Musfeldt *et al.*, 2013). The monoclinic β-angle increases continuously up to 4.2 GPa, with the largest changes occurring immediately after the transition (91–96° in the range 1–2 GPa). While the *a*-axis shows a slightly decreasing trend in absolute value, the change to monoclinic symmetry and large changes in the β-angle result in a comparable NLC effect [$-4.1\,(4)\ \mathrm{TPa}^{-1}$] that is now approximately aligned with the 'long' *ac* diagonal (Fig. S3). The linear compressibility in the orthogonal directions (along *b* and approximately along the 'short' *ac* diagonal) are both positive with values of $\sim 23\ \mathrm{TPa}^{-1}$ (Fig. S5).

4.2. Mechanism of the α-Co(dca)$_2$ to γ-Co(dca)$_2$ transformation

At close to ambient pressure the structural parameters for α-Co(dca)$_2$ are consistent with the previously reported single-crystal structure, with equatorial Co—N (cyanide) and axial Co—N (amide) bond lengths that are approximately equal (~ 2.1 Å), and an amide C—N—C bond angle of $\sim 117°$ (Kurmoo & Kepert, 1998). Upon increasing pressures approaching the phase transformation (1.1 GPa) there is a dramatic increase in the axial Co—N bond length, while the equatorial distances remain relatively constant (Fig. 4*a*). At pressures close to the transition the axial Co—N bond length becomes significantly larger than the range of typical Co—N coordination bond lengths (1.84–2.19 Å). According to data available from the Cambridge Structure Database (Version 5.35 plus one update; 1.84–2.19 Å; Allen, 2002), these values suggest a shift from a traditional coordination bond toward a more van der Waals-like interaction. This appears somewhat counterintuitive given the changes in lattice parameters discussed above which show NLC along the chain direction that should correlate to the lengthening of the equatorial Co—N bond distances. However, over the same pressure range there is an increase in the amide C—N—C bond angle to values $> 130°$ close to the transition pressure (Fig. 4*b*). At 1.1 GPa, these perturbations become sufficiently large that the mirror plane symmetry can no longer be sustained while still providing overall volume compression, thereby triggering the α-Co(dca)$_2$ to γ-Co(dca)$_2$ phase transformation. The transition allows the axial Co—N bond lengths to relax to values again similar to the equatorial bonds (~ 2.1 Å), while the C—N—C angle retains a moderately strained value of 130° up to the maximum measured pressure. This strain is presumably a contributing factor in the reversibility of the structural transition.

In contrast to high-pressures studies of the molecular magnet $CuF_2(H_2O)_2$(pyrazine), where the mechanism for volume conserving structural transitions was attributed to distortion within the Cu^{II} octahedra (Halder *et al.*, 2011), in the present study the Co^{II} octahedra remain relatively rigid (Fig. S6*a*). However, significant rotation of the octahedra are observed for γ-Co(dca)$_2$ (Fig. 5*a*). This rotation is also apparent in the Co—N$_{eq}$—C angles which steadily decrease with pressure from $\sim 160°$ at ambient pressure to $\sim 140°$ at 4 GPa (Fig. S6*b*). Asymmetry in the coordination bond orientation between the two distinct cyanide groups in γ-Co(dca)$_2$ is likely an important factor in the materials adaptability to extreme pressures, with larger changes observed for the Co—N3—C2 bond compared with that of Co—N1—C1 at pressures above 3 GPa.

4.3. Impact of the α-Co(dca)$_2$ to γ-Co(dca)$_2$ transformation on magnetic properties

The observed structural transformation from α-Co(dca)$_2$ to γ-Co(dca)$_2$ occurs at a similar pressure (~ 1 GPa) to the previously reported magnetic crossover from ferromagnetic to antiferromagnetic behaviour (Nuttall *et al.*, 2000). There are several pathways for nearest-neighbour exchange interactions, with earlier work showing that between different members of the rutile-like α-M^{II}(dca)$_2$ family the magnetic exchange interactions are highly dependent on the *M*—N bond distances and structural distortions (Kurmoo & Kepert, 1998). However, it is expected that the highest magnitude exchange pathways for α-Co(dca)$_2$ are those along the most direct diagonal (J_d) linkages between Co^{II} centres on adjacent chains (*i.e.* ···Co—N≡C—N—Co···), particularly in comparison to those along the chains [*i.e.* ···Co—(N≡C—N—C≡N)—Co···]. The pressure-dependent structure for α-Co(dca)$_2$ shows much greater compressibility in the *b* and *c* directions (perpendicular to the chain direction), which might be expected to enhance J_d by reducing the Co···Co distance. This is in agreement with the magnetic investigations where the Curie temperature increases with applied pressure below 1 GPa (Nuttall *et al.*, 2000). Presumably, the pronounced rotation of the Co^{II} octahedra in the high-pressure phase, γ-Co(dca)$_2$, has a major impact on these exchange pathways and is likely a critical factor in the ferromagnetic to antiferromagnetic crossover.

5. Conclusion

The pressure-induced structural transformation of α-Co(dca)$_2$ to the high-pressure phase γ-Co(dca)$_2$ has been probed using synchrotron powder diffraction. Detailed crystallographic analyses revealed a mechanism for the transition as well as a range of structural perturbations that contribute volume-conserving effects at high pressures. The mechanism is driven by a combination of destabilizing factors within α-Co(dca)$_2$, including the elongation of the Co^{II} octahedral and strain on the amide bond angle of the ligand. The reduction in symmetry for γ-Co(dca)$_2$ not only allows for a tilting effect in the crystal packing, but also asymmetry in the coordination binding geometries of the cyanide groups of the ligands and a pronounced rotation of the Co^{II} octahedral at high pressures. This work demonstrates that pressure offers a novel approach for generating new phases and exploring the structure–property relationships of molecular materials. Our future work will involve investigations of the pressure-dependent structures of further transition metal dicyanamides, including members of the iso-structural α-M^{II}(dca)$_2$ family as well as other polymorphs, to uncover any universality or metal-ion dependence

associated with the $\alpha \rightarrow \gamma$ transition, and if other new phases can be generated.

Acknowledgements

This research used resources of the Advanced Photon Source, a US Department of Energy (DOE) Office of Science User Facility operated for the DOE Office of Science by Argonne National Laboratory (ANL) under Contract No. DE-AC02-06CH11357. AAY thanks the Director's Postdoctoral Fellowship program at ANL.

References

Allen, F. H. (2002). *Acta Cryst.* B**58**, 380–388.
Anthony, J. W., Bideaux, R. A., Bladh, K. W. & Nichols, M. C. (2001). *Handbook of Mineralogy*. Chantilly, USA: Mineralogical Society of America.
Batten, S. R., Robson, R., Jensen, P., Moubaraki, B. & Murray, K. S. (1998). *Chem. Commun.* pp. 439–440.
Bennett, T. D., Simoncic, P., Moggach, S. A., Gozzo, F., Macchi, P., Keen, D. A., Tan, J.-C. & Cheetham, A. K. (2011). *Chem. Commun.* **47**, 7983–7985.
Cairns, A. B., Catafesta, J., Levelut, C., Rouquette, J., van der Lee, A., Peters, L., Thompson, A. L., Dmitriev, V., Haines, J. & Goodwin, A. L. (2013). *Nat. Mater.* **12**, 212–216.
Chapman, K. W., Halder, G. J. & Chupas, P. J. (2008). *J. Am. Chem. Soc.* **130**, 10524–10526.
Chapman, K. W., Halder, G. J. & Chupas, P. J. (2009). *J. Am. Chem. Soc.* **131**, 17546–17547.
Chapman, K. W., Sava, D. F., Halder, G. J., Chupas, P. J. & Nenoff, T. M. (2011). *J. Am. Chem. Soc.* **133**, 18583–18585.
Cliffe, M. J. & Goodwin, A. L. (2012). *J. Appl. Cryst.* **45**, 1321–1329.
Decker, D. L. (1971). *J. Appl. Phys.* **42**, 3239–3244.
Furukawa, H., Cordova, K. E., O'Keeffe, M. & Yaghi, O. M. (2013). *Science*, **341**, 1230444.
Goodwin, A. L., Keen, D. A. & Tucker, M. G. (2008). *Proc. Natl Acad. Sci. USA*, **105**, 18708–18713.
Graham, A. J., Allan, D. R., Muszkiewicz, A., Morrison, C. A. & Moggach, S. A. (2011). *Angew. Chem. Int. Ed.* **50**, 11138–11141.
Halder, G. J., Chapman, K. W., Schlueter, J. A. & Manson, J. L. (2011). *Angew. Chem. Int. Ed.* **50**, 419–421.
Hammersley, A. P., Svensson, S. O., Hanfland, M., Fitch, A. N. & Hausermann, D. (1996). *High. Press. Res.* **14**, 235–248.
Jensen, P., Batten, S. R., Fallon, G. D., Moubaraki, B., Murray, K. S. & Price, D. J. (1999). *Chem. Commun.* pp. 177–178.
Köhler, H. (1964). *Z. Anorg. Allg. Chem.* **331**, 237–248.
Kurmoo, M. (2009). *Chem. Soc. Rev.* **38**, 1353–1379.
Kurmoo, M. & Kepert, C. J. (1998). *New J. Chem.* **22**, 1515–1524.
Lapidus, S. H., Halder, G. J., Chupas, P. J. & Chapman, K. W. (2013). *J. Am. Chem. Soc.* **135**, 7621–7628.
Li, W., Probert, M. R., Kosa, M., Bennett, T. D., Thirumurugan, A., Burwood, R. P., Parinello, M., Howard, J. A. K. & Cheetham, A. K. (2012). *J. Am. Chem. Soc.* **134**, 11940–11943.
Marquardt, D. W. (1963). *J. Soc. Ind. Appl. Math.* **11**, 431–441.
Musfeldt, J. L., Brinzari, T. V., Schlueter, J. A., Manson, J. L., Litvinchuk, A. P. & Liu, Z. (2013). *Inorg. Chem.* **52**, 14148–14154.
Nuttall, C. J., Takenobu, T., Iwasa, Y. & Kurmoo, M. (2000). *Mol. Cryst. Liq. Cryst. Sci. Technol. Sect. A*, **343**, 227–234.
Ogborn, J. M., Collings, I. E., Moggach, S. A., Thompson, A. L. & Goodwin, A. L. (2012). *Chem. Sci.* **3**, 3011–3017.
Petříček, V., Dusek, M. & Palatinus, L. (2006). *JANA*2006. Praha, Czech Republic, Institute of Physics.
Piermarini, G. J. (1973). *J. Appl. Phys.* **44**, 5377–5382.
Tan, J. C. & Cheetham, A. K. (2011). *Chem. Soc. Rev.* **40**, 1059–1080.
Toby, B. H. & Von Dreele, R. B. (2013). *J. Appl. Cryst.* **46**, 544–549.